

Hierarchical Probabilistic Model for Blind Source Separation via Legendre Transformation

Simon Luo

The University of Sydney
sluo4225@uni.sydney.edu.au

Lamia Azizi

The University of Sydney
lamiae.azizi@sydney.edu.au

Mahito Sugiyama

National Institute of Informatics
mahito@nii.ac.jp

Abstract

We present a novel *blind source separation* (BSS) method, called *information geometric blind source separation* (IG-BSS). Our formulation is based on the information geometric log-linear model equipped with a hierarchically structured sample space, which has theoretical guarantees to uniquely recover a set of source signals by minimizing the KL divergence from a set of mixed signals. Source signals, received signals, and mixing matrices are realized as different layers in our hierarchical sample space. Our empirical results have demonstrated on images that our approach is superior to current state-of-the-art techniques and is able to separate signals with complex interactions.

Introduction

The objective of *Blind source separation* (BSS) is to identify a set of source signals from a set of multivariate mixed signals¹. BSS is widely used for applications which are considered to be the “cocktail party problem”. Examples include image/signal processing (Isomura and Toyoizumi 2016), artifact removal in medical imaging (Vigário et al. 1998) and electroencephalogram (EEG) signal separation (Congedo, Gouy-Pailler, and Jutten 2008).

Currently, there are a number of solutions for the BSS problem. However they all have limitations with their approaches. The most widely used approaches are variations of principal component analysis (PCA) (Pearson 1901; Murphy 2012) and independent component analysis (ICA) (Comon 1994; Murphy 2012).

PCA and its more modern variations such as sparse PCA (SPCA) (Zou, Hastie, and Tibshirani 2006), non-linear PCA (NLPCA) (Scholz et al. 2005) and Robust PCA (Xu, Caramanis, and Sanghavi 2010) extract a specified number of components with the largest variance under an orthogonal constraint, where the resulting components are composed of a linear combination of the variables. They create a set of uncorrelated orthogonal basis vectors that represent the source signal. The basis vectors with the N largest variance

are called the principal components and is the output of the model. PCA has shown to be effective for many applications such as dimensionality reduction and feature extraction. However, for BSS, PCA makes the assumption that the source signals are orthogonal, which is often not the case in most practical applications.

Similarly, ICA also attempts to find the N components with the largest variance, but relaxes the orthogonality constraint. All variations of ICA such as infomax (Bell and Sejnowski 1995), FastICA (Hyvärinen and Oja 2000) and JADE (Cardoso 1999) separate a multivariate signal into additive subcomponents by maximizing statistical independence of each component. ICA assumes that each component is non-gaussian and the relationship between the source signal and the mixed signal is an affine transformation. In addition to these assumptions, ICA is sensitive to the initialization of the weights as the optimization is non-convex and is likely to converge to a local optimum.

Other potential methods which can perform BSS include non-negative matrix factorization (NMF) (Lee and Seung 2001; Berne et al. 2007) and dictionary learning (DL) (Olshausen and Field 1997). NMF and DL are not widely used in BSS as they lose information when recovering the source signal from the mixed signal. NMF factorizes a matrix into two matrices with nonnegative elements representing weights and features. The features extracted by NMF can be used to recover the source signal. NMF may perform well on signals which have only positive values such as images. However, NMF does not maximize statistical independence which is required to completely separate the mixed signal into the source signal, and it is also sensitive to initialization as the optimization is non-convex. Due to the non-convexity, additional constraints or heuristics for weight initialization is often applied to NMF to achieve better results (Ding, Li, and Jordan 2008; Boutsidis and Gallopoulos 2008). DL can be thought of as a variation of the ICA approaches which requires an over-complete basis vector for the mixing matrix. DL may be advantageous because additional constraints such as a positive code or a dictionary can be applied to the model. However, since it requires an over-complete basis vector, information may be lost when reconstructing the source signal. In addition, like all other approaches, DL is

also non-convex making sensitive to the initialization of the weights.

All previous approaches have limitations such as loss of information or non-convex optimization and require constraints or assumptions such as orthogonality and an affine transformation which are not ideal for BSS. In the following we introduce our approach to BSS by using an *information geometric formulation of the log-linear model*. Unlike the previous approaches, our proposed approach does not have the assumptions or limitations that they require. We provide a flexible solution by introducing a *hierarchical structure* between signals into our model, which allows us to treat interactions between signals that are more complex than an affine transformation. Our experimental results demonstrate that our hierarchical model leads to better separation of signals including complex interaction such as higher-order feature interactions (Luo and Sugiyama 2019) than existing methods. Our method solves a convex optimization problem, hence it always arrives at the globally optimal unique solution. Moreover, we theoretically show that it always minimizes the Kullback–Leibler (KL) divergence from a set of mixed signals to a set of source signals.

Formulation

BSS is mathematically defined as a function f which is able to separate a set of *mixed signals* X into a set of *source signals* Z , i.e., $Z = f(X)$. However, it is generally considered to be impossible for the function f to recover the scale and the original order of the source signal. If we apply this limitation to the BSS problem, the problem is mathematically reduced to $Z \propto f(X)$.

We will first introduce background on the traditional formulation of ICA. We then introduce the information geometric formulation of the log-linear model, which is the foundation of our proposal. This is then followed by our proposed model, information geometric formulation of blind source separation (IGBSS), by introducing a hierarchical structure into the sample space of the log-linear model. Finally, we introduce the optimization of IGBSS.

Independent Component Analysis

Let $\mathbf{Z} = [\mathbf{z}_1, \dots, \mathbf{z}_M]$, $\mathbf{z}_m \in \mathbb{R}^N$ be a set of *source signals* and $\mathbf{X} = [\mathbf{x}_1, \dots, \mathbf{x}_M]$, $\mathbf{x}_m \in \mathbb{R}^L$ be a set of *received signals*. The received signal \mathbf{X} is an affine transformation of the source signal \mathbf{Z} by a *mixing matrix* $\mathbf{A} \in \mathbb{R}^{L \times N}$: $\mathbf{A} = [\mathbf{a}_1, \dots, \mathbf{a}_N]$, written as

$$\mathbf{X} = \mathbf{AZ}, \quad x_{lm} = \sum_{n=1}^N a_{ln} z_{nm}, \quad (1)$$

where L is the number of received signals, N is the number of source signals and M is the sample size. The source signal can be recovered from \mathbf{A} and \mathbf{X} if $L \geq N$, while the source signal \mathbf{Z} and the mixing matrix \mathbf{A} are unknown in BSS. Our objective is to estimate the source signal \mathbf{Z} by learning the parameters in \mathbf{A} using the received signal \mathbf{X} as the input to the model. The traditional formulation of ICA aims to learn the inverse of \mathbf{A} . Differently, our approach is able to learn the equivalent for the parameters of \mathbf{A} directly.

Information Geometric Formulation of the Log-Linear Model with Hierarchical Structure

We introduce the information geometric formulation of the *log-linear model* proposed by Sugiyama *et al.* (Sugiyama, Nakahara, and Tsuda 2016; Sugiyama, Nakahara, and Tsuda 2017). Let Ω be the sample space of a discrete probability distribution P , where we assume that Ω is a *partially ordered set* (Davey and Priestley 2002), that is, Ω is equipped with a partial order \leq . The space Ω contains at least one element which is known as the least element denoted as \perp , i.e., $\perp \leq \omega$ for all $\omega \in \Omega$, and we denote by $\Omega^+ = \Omega \setminus \{\perp\}$. A predetermined subset $\mathcal{S} \subseteq \Omega^+$ is used as the domain of parameters of the log-linear model, and a real-valued parameter $\theta(s) \in \mathbb{R}$ is given for each $s \in \mathcal{S}$. We then define probability $p(\omega; \theta)$ for each element ω given parameters θ in the log-linear model as follows:

$$\log p(\omega; \theta) = \sum_{s \in \mathcal{S}, s \leq \omega} \theta(s) - \psi(\theta), \quad (2)$$

where $\psi(\theta) \in \mathbb{R}$ is the partition function which is uniquely determined from the parameters $(\theta(s))_{s \in \mathcal{S}}$,

$$\psi(\theta) = \log \sum_{\omega \in \Omega} \prod_{s \in \mathcal{S}, s \leq \omega} \exp(\theta(s)) = -\theta(\perp). \quad (3)$$

A special case of the joint density function in Equation (2) is known to coincide with the *Boltzmann machine* (Sugiyama, Nakahara, and Tsuda 2018; Luo and Sugiyama 2019). The expectation for each $\omega \in \Omega$, denoted by $\eta(\omega; \theta)$, is given as

$$\eta(\omega; \theta) = \sum_{\omega' \in \Omega, \omega' \geq \omega} p(\omega'; \theta), \quad (4)$$

and the pair $((\theta(\omega))_{\omega \in \Omega^+}, (\eta(\omega))_{\omega \in \Omega^+})$ is connected via *Legendre transformation* and forms a *dual coordinate system* of the set of distributions $\mathfrak{S} = \{P \mid 0 < p(\omega) < 1 \text{ and } \sum_{\omega \in \Omega} p(\omega) = 1\}$ with respect to the sample space Ω (Sugiyama, Nakahara, and Tsuda 2017, Theorem 2). This means that \mathfrak{S} becomes a *dually flat Riemannian manifold*, which is the standard manifold in information geometry (Amari 2016).

We use the information geometric formulation of the log-linear model as the foundation for our proposed approach to achieve BSS.

Information Geometric Formulation of Blind Source Separation

Here we introduce our key technical contribution of this paper, a hierarchical structure for the sample space Ω of the log-linear model, to achieve BSS. We call this model *information geometric BSS* (IGBSS). In the following, we treat a received (mixed) signal \mathbf{X} as a discrete probability mass function by normalizing it by dividing each element by the sum of all elements. We prepare $\omega_{x_{11}}, \dots, \omega_{x_{LM}}$ as elements of the sample space Ω and each normalized entry $x_{lm} / \sum_{lm} x_{lm}$ of the original input \mathbf{X} as its probability $p(\omega_{x_{lm}})$. The number of source signals N is also a fixed input to the model.

We define the sample space to be $\Omega = \{\perp\} \cup \mathcal{A} \cup \mathcal{Z} \cup \mathcal{X}$, where $\mathcal{A} = \{\omega_{a_{11}}, \dots, \omega_{a_{LN}}\}$, $\mathcal{Z} = \{\omega_{z_{11}}, \dots, \omega_{z_{MN}}\}$, and

Bottom Node The bottom node \perp provides the connections for all the elements in the node. The θ value $\theta(\perp)$ is the negative of the partition function, i.e., $\psi(\theta) = -\theta(\perp)$. The partition function ensures the entire outcome space sums to 1, that is, $\sum_{\omega \in \Omega} p(\omega) = 1$. The partition function is not necessarily when the model is applied to perform BSS.

Optimization

We optimize our log-linear model by minimizing the KL divergence from an empirical distribution \hat{P} to the model distribution P . Given a received signal X as an input dataset. The empirical distribution \hat{P} is defined as $\hat{p}(x_{ij}) = x_{ij} / \sum_{ij} x_{ij}$ for all $x_{ij} \in \mathcal{X}$, $\hat{p}(z) = 0$ for all $z \in \mathcal{Z}$, and $\hat{p}(a) = 0$ for all $a \in \mathcal{A}$. The empirical expectation $\hat{\eta}(\omega)$ for each layer can be computed by using the values of the empirical distribution \hat{P} with Equation (6), Equation (8) and Equation (10) for the received, source and mixed layer respectively.

Let us introduce two submanifolds of the set of distributions \mathfrak{S} of our log-linear model. They are given as $\mathfrak{S}_\theta = \{P \in \mathfrak{S} \mid \theta(\omega) = 0, \forall \omega \in \Omega^+ \setminus S\}$, which is an e -flat submanifold with θ coordinates, and $\mathfrak{S}_\eta = \{P \in \mathfrak{S} \mid \eta(\omega) = \hat{\eta}(\omega), \forall \omega \in S\}$, which is an m -flat submanifold with η coordinates. The intersection $\mathfrak{S}_\theta \cap \mathfrak{S}_\eta$ is always a singleton and it always minimizes the KL divergence (Amari 2009, Theorem 3), that is, it is the globally optimal solution of our model.

To find the solution, we perform e -projection, which projects a probability distribution in \mathfrak{S}_θ onto \mathfrak{S}_η . The e -projection is always a convex optimization as the e -flat submanifold \mathfrak{S}_η is convex with respect to $(\theta_\omega)_{\omega \in \Omega^+}$ (Amari 2016). The KL divergence from a given empirical distribution \hat{P} to a model distribution P is written as

$$D_{\text{KL}}(\hat{P} \| P) = \sum_{\omega \in \Omega} \hat{p}(\omega) \log \frac{\hat{p}(\omega)}{p(\omega)} \quad (11)$$

$$= - \sum_{\omega \in \Omega} \hat{p}(\omega) \log p(\omega) - \mathbb{H}(\hat{P}), \quad (12)$$

where $\mathbb{H}(\hat{P}) = - \sum_{\omega \in \Omega} \hat{p}(\omega) \log \hat{p}(\omega)$ is the entropy of \hat{P} and independent of $(\theta_\omega)_{\omega \in \Omega^+}$, hence it can be dropped for optimization. Since we have

$$- \sum_{\omega \in \Omega} \hat{p}(\omega) \log p(\omega) = \sum_{\omega \in \Omega} \hat{p}(\omega) \left[- \sum_{s \in S} \theta(s) + \psi(\theta) \right], \quad (13)$$

$$\psi(\theta) = - \log \sum_{\omega \in \Omega} \exp \left[\sum_{s \in S} \theta(s) \right], \quad (14)$$

we can confirm that $D_{\text{KL}}(\hat{P} \| P)$ is convex with respect to $(\theta_\omega)_{\omega \in \Omega^+}$. We take the derivative with respect to $\theta(s)$ to obtain the gradient for each update step, given as

$$\frac{\partial}{\partial \theta(s)} D_{\text{KL}}(\hat{P} \| P) = - \frac{\partial}{\partial \theta(s)} \sum_{\omega \in \Omega} \hat{p}(\omega) \log p(\omega) \quad (15)$$

$$= \frac{\partial}{\partial \theta(s)} \sum_{\omega \in \Omega} \hat{p}(\omega) \left[- \sum_{s' \in S} \theta(s') + \psi(\theta) \right] \quad (16)$$

$$= \frac{\partial}{\partial \theta(s)} \sum_{\omega \in \Omega} \hat{p}(\omega) \psi(\theta) - \frac{\partial}{\partial \theta(s)} \sum_{\omega \in \Omega} \hat{p}(\omega) \sum_{s' \in S} \theta(s') \quad (17)$$

$$= \frac{\partial}{\partial \theta(s)} \psi(\theta) - \sum_{\omega \in \Omega} \hat{p}(\omega) \mathbb{I}(\omega \leq s) \quad (18)$$

$$= \eta(s) - \hat{\eta}(s) = \Delta \eta(s) \quad (19)$$

where we have used the fact that $\partial \psi(\theta) / \partial \theta(s) = \eta(s)$ as shown in (Sugiyama, Nakahara, and Tsuda 2017, Theorem 2). This equation shows that the KL divergence $D_{\text{KL}}(\hat{P}, P)$ is minimized if and only if $\eta(s) = \hat{\eta}(s)$ for all $s \in S$.

From Equation (10), the gradient for the mixing layer is given as

$$\frac{\partial}{\partial \theta(a)} D_{\text{KL}}(\hat{P} \| P) = \eta(a) - \hat{\eta}(a) \quad (20)$$

$$= \left[\sum_{x \in \mathcal{X}, x \geq a} p(x) + \sum_{z \in \mathcal{Z}, z \geq a} p(z) + p(a) \right] - \sum_{x \in \mathcal{X}, x \geq z} \hat{p}(x). \quad (21)$$

Likewise, for the source layer we obtain the gradient from Equation (8):

$$\frac{\partial}{\partial \theta(z)} D_{\text{KL}}(\mathcal{P} \| Q) = \eta(z) - \hat{\eta}(z) \quad (22)$$

$$= \left[\sum_{x \in \mathcal{X}, x \geq z} p(x) + p(z) \right] - \sum_{x \in \mathcal{X}, x \geq z} \hat{p}(x). \quad (23)$$

Using the above results, gradient descent can be directly applied for the convex optimization problem and can solve our e -projection. However, this may need a large number of iterations to reach convergence. To reduce the number of iterations, we proposed to use *natural gradient* (Amari 1998) which is a second-order optimization approach. The natural gradient is an instance of the *Bregman algorithm* applied to convex regions and is well known that it is able to converge to the global optimal solution (Censor and Lent 1981). In our optimization problem, we are able to find the global optimal solution using natural gradient because the KL divergence $D_{\text{KL}}(\mathcal{P} \| Q)$ is convex. We formulate the natural gradient by letting $\theta = [\theta(s_1), \dots, \theta(s_{|S|})]^T$ and $\eta = [\eta(s_1), \dots, \eta(s_{|S|})]^T$. In each update of the current θ to θ_{next} , the natural gradient method uses the relationship $\Delta \eta = -\mathbf{G} \Delta \theta$, $\Delta \eta = \eta - \hat{\eta}$ and $\Delta \theta = \theta_{\text{next}} - \theta$ which leads to the update step

$$\theta_{\text{next}} = \theta - \mathbf{G}^{-1} \Delta \eta, \quad (24)$$

where $\mathbf{G} = (g_{ss'}) \in \mathbb{R}^{|S| \times |S|}$ is the Fisher information matrix such that

$$g_{ss'}(\theta) = \frac{\partial \eta(s)}{\partial \theta(s')} = \mathbb{E} \left[\frac{\partial \log p(\omega)}{\partial \theta(s)} \frac{\partial \log p(\omega)}{\partial \theta(s')} \right] \quad (25)$$

$$= \sum_{\omega \in \Omega, \omega \geq s, \omega \geq s'} p(\omega) - \eta(s) \eta(s') \quad (26)$$

This equation (26) is obtained from Theorem 3 in (Sugiyama, Nakahara, and Tsuda 2017). The natural gradient coincides with Newton's method in our case as the Fisher information matrix \mathbf{G} corresponds to the negative Hessian matrix,

$$\frac{\partial}{\partial \theta(s) \partial \theta(s')} D_{\text{KL}}(\hat{P} \| P) = - \frac{\partial \eta(s)}{\partial \theta(s')} = -g_{ss'}. \quad (27)$$

Algorithm 1: Information Geometric BSS

```

1 Function IGBSS( $\hat{P}, S$ ):
2   Initialize  $(\theta(s))_{s \in S}$  (randomly or  $\theta(s) = 0$ )
3   repeat
4     Compute  $P$  using the current parameter
        $(\theta(s))_{s \in S}$ 
5     Compute  $(\eta(\omega))_{\omega \in \Omega^+}$  from  $P$ 
6      $(\Delta\eta(\omega))_{\omega \in \mathcal{Z}} \leftarrow (\eta(\omega))_{\omega \in \mathcal{Z}} - (\hat{\eta}(\omega))_{\omega \in \mathcal{Z}}$ 
7      $(\Delta\eta(\omega))_{\omega \in \mathcal{A}} \leftarrow (\eta(\omega))_{\omega \in \mathcal{A}} - (\hat{\eta}(\omega))_{\omega \in \mathcal{A}}$ 
8     Compute the Fisher information matrix for
       source layer  $\mathbf{G}_Z$  and the mixing layer  $\mathbf{G}_A$ 
9      $(\theta(\omega))_{\omega \in \mathcal{Z}} \leftarrow (\theta(\omega))_{\omega \in \mathcal{Z}} - \mathbf{G}_Z^{-1}(\Delta\eta(\omega))_{\omega \in \mathcal{Z}}$ 
10     $(\theta(\omega))_{\omega \in \mathcal{A}} \leftarrow (\theta(\omega))_{\omega \in \mathcal{A}} - \mathbf{G}_A^{-1}(\Delta\eta(\omega))_{\omega \in \mathcal{A}}$ 
11  until convergence of  $(\theta(s))_{s \in S}$ 

```

Inverting a matrix is computationally expensive and has a complexity of $\mathcal{O}(|S|^3)$. In IGBSS, the entries for the cross-layer interaction between the mixing layer and the source layer are always $g_{az} = g_{za} = 0$ for all $a \in \mathcal{A}$ and $z \in \mathcal{Z}$. Hence they can be ignored in optimization. To improve the efficiency of optimization, we separate the update steps in the source layer and the mixing layer, that is,

$$(\theta_{\text{next}})_{\omega \in \mathcal{Z}} = (\theta)_{\omega \in \mathcal{Z}} - \mathbf{G}_Z^{-1}(\Delta\eta)_{\omega \in \mathcal{Z}}, \quad (28)$$

$$(\theta_{\text{next}})_{\omega \in \mathcal{A}} = (\theta)_{\omega \in \mathcal{A}} - \mathbf{G}_A^{-1}(\Delta\eta)_{\omega \in \mathcal{A}}, \quad (29)$$

where \mathbf{G}_Z^{-1} and \mathbf{G}_A^{-1} are the Fisher information matrix for the source layer and mixing layer, respectively. They are constructed by assuming all other parameters are fixed. This approach reduces the complexity of the model to $\mathcal{O}(|\mathcal{Z}|^3 + |\mathcal{A}|^3)$. In most practical cases, the size of $|\mathcal{Z}|$ is much greater than $|\mathcal{A}|$. This implies that the complexity of the model does not increase significantly if we include higher-order feature interactions. The full Algorithm using natural gradient is given in Algorithm 1. The complexity to compute Q in Algorithm 1 Line 5 is $\mathcal{O}(|\Omega||S|)$. The complexity to compute $\Delta\eta$ in Algorithm 1 Line 6 and Line 7 is $\mathcal{O}(|\mathcal{Z}|) + \mathcal{O}(|\mathcal{A}|) = \mathcal{O}(|S|)$. Therefore the total complexity of the model for each iteration is $\mathcal{O}(|\mathcal{Z}|^3 + |\mathcal{A}|^3 + |\Omega||S|)$.

Experiments

We empirically examine the effectiveness of IGBSS to perform BSS using real-world datasets for an affine transformation and higher-order interactions between signals. We also evaluate efficiency of IGBSS.

Blind Source Separation for Affine Transformations

We demonstrate the effectiveness of our model. In our experiments, we use three benchmark images widely used in computer vision from the University of Southern California's Signal and Image Processing Institute (USC-SIPi)², which include "airplane (F-16)", "lake" and "peppers". Each image is standardized to have 32x32 pixels with red, green

Table 1: RMSE of the euclidean distance between the reconstruction and the ground truth. (*) Experimental results for Figure 2. (†) Experimental results for Figure 3. Each run of the experiment contains a different set of images and a new randomly generated mixing matrix.

Exp.	Order	IGBSS	FastICA	NMF	DL
1	First*	0.27032	0.43630	0.62195	0.37167
	Second	0.23215	0.33516	0.66241	0.50457
	Third†	0.19945	0.41677	0.61145	0.52153
2	First	0.24263	0.39704	0.59142	0.46789
	Second	0.22961	0.56500	0.68390	0.58742
	Third	0.20848	0.62999	0.66455	0.60256
3	First	0.26299	0.44945	0.63427	0.47442
	Second	0.21221	0.33055	0.71056	0.58540
	Third	0.18630	0.39838	0.67965	0.61310

and blue color channels with integer values between 0 and 255 to represent the intensity of each pixel. These images shown in Figure 2a are the *source signal* \mathbf{Z} which are unknown to the model. They are only used as ground truth to evaluate the model output. Equation (1) is used to generate the received signal \mathbf{X} by randomly generating values for a mixing matrix \mathbf{A} using the uniform distribution which generates real numbers between 1 and 6. The images are then rescaled to integer values within the range between 0 and 255. The received signal \mathbf{X} , which is the input to the model, is the three images shown in Figure 2b. The three images for the mixed signal may look visually similar, however, they are actually superposition of the source signal with different intensity. The objective of our model is to reconstruct the *source signal* \mathbf{Z} without knowing the *mixing matrix* \mathbf{A} .

We compare our approach to FastICA with the log cosh function as the signal prior, DL with constraint for positive dictionary and positive code, and NMF with the coordinate descent solver and non-negative double singular value decomposition (NNDSVD) initialization (Boutsidis and Gallopoulos 2008) with zero values replaced with the mean of the input. Since the order of the signal is not recovered, take all permutations of the output and calculate the minimum euclidean distance with the ground truth. The permutation which returns the minimum error is considered the correct order of the image. The scale of the output is also not recovered, we have used min-max normalize the output of each model using $z_{\text{norm}} = (z_{\text{out}} - \min(z_{\text{out}})) / (\max(z_{\text{out}}) - \min(z_{\text{out}}))$.

We visually inspect each of the model output and compare it to the ground truth. Our proposed approach IGBSS is able to recover majority of the "shape" of the source signal, while the intensity of each image appears to larger than the ground truth for all images. Small residuals of each image can be seen on the other images. For instance, in the airplane (F-16) image, there residuals from the lake image can be clearly seen. Compared to the reconstruction of IGBSS with FastICA, DL and NMF, IGBSS performs significantly better as all other approaches are unable to clearly separate the mixed signal. FastICA was unable to provide a reason-

²<http://sipi.usc.edu/database/>



(a) Source signal (ground truth).



(b) Received signal (input).



(c) Reconstructed signal using IGBSS.



(d) Reconstructed Signal using FastICA.



(e) Reconstructed signal using dictionary learning with positive dictionary and positive code.



(f) Reconstructed signal using non-negative matrix factorization.

Figure 2: First-order interaction experiment. Number of source signal: 3, order of interaction: 1, Number of mixed signal: 3.



(a) Source signal (ground truth).



(b) Received signal (input).



(c) Reconstructed signal using IGBSS.



(d) Reconstructed Signal using FastICA.



(e) Reconstructed signal using dictionary learning with positive dictionary and positive code.



(f) Reconstructed signal using non-negative matrix factorization.

Figure 3: Higher-order interaction experiment. Number of source signal: 3, order of interaction: 3, Number of mixed signal: 3.

able reconstruction with 3 mixed signal. To overcome this limitation of FastICA, we randomly generated another column of the mixing matrix and append it to the current mixing matrix to create 4 mixed signals as an input to FastICA to recover a more reasonable signal.

To quantify results of BSS, we calculated the root mean square error (RMSE) of the Euclidean distance between the reconstruction and the ground truth. The full results are shown in Table 1 (top row for each experiment). In the table, we present three experiments with different RGB images from USC-SIPI dataset, for each experiment we generate a new mixing matrix, where the second and the third experiments uses images of “mandrill”, “splash”, “jelly beans” and “mandrill”, “lake”, “peppers”, respectively. Ground truth and resulting images for second and third experiments are presented in Supplement.

Our results clearly show that IGBSS is superior to other methods, that is, IGBSS has consistently produced the lowest error for every experiment.

Blind Source Separation with Higher-Order Feature Interactions

We demonstrate the ability of BSS for our model to include *higher-order features interactions* in BSS. We use the same benchmark images in the standard BSS as the *source signal* \mathbf{Z} for our experiment. We generate the higher-order feature interactions of the *received signal* by using the multiplicative product of the *source signal*. That is, $x_{lm} = \sum_{n=1}^N a_{ln} z_{nm} + \sum_{n=1}^N a_{ln} z_{nm} z_{nm'} + \sum_{n=1}^N a_{ln} z_{nm} z_{nm'} z_{nm''} + \dots + \sum_{n=1}^N a_{ln} z_{nm} z_{nm'} \dots z_{nm'} \dots$. All the other known approaches take into account only first order interactions (that is, affine transformation) between features. Differently, our model can directly incorporate the higher-order features as we do not have any assumption of the affine transformation. Figure 3 shows experimental results for the higher-order feature experiment. Our approach IGBSS shows superior reconstruction of the source signal to other approaches. All the other approaches except for NMF is able to achieve reasonable reconstruction. NMF is able to recover the “shape” of the image, however, unlike IBSS, NMF is unable to recover all color channels in the correct proportion, creating discoloring for the image. Since the proportion of the intensity of the pixel is not recovered. In terms of the RMSE shown in Table 1, IGBSS again shows the best results for both second- and third-order interactions of signals across three experiments.

Runtime Analysis

We have designed experiments to confirm the runtime of the model. Figure 4 confirms that the runtime for both natural gradient and gradient descent is less than exponential. Although the time complexity for each iteration of natural gradient is $O(|\mathbf{Z}|^3 + |\mathcal{A}|^3 + |\Omega||S|)$, which is larger than $O(|\Omega||S|^2)$ for gradient descent, natural gradient is able to reach convergence faster because it is quadratic convergence and requires significantly less iterations compared to gradient descent, which linearly converges. Increasing the size of the input will increase the size of $|\Omega|$ only, while the number

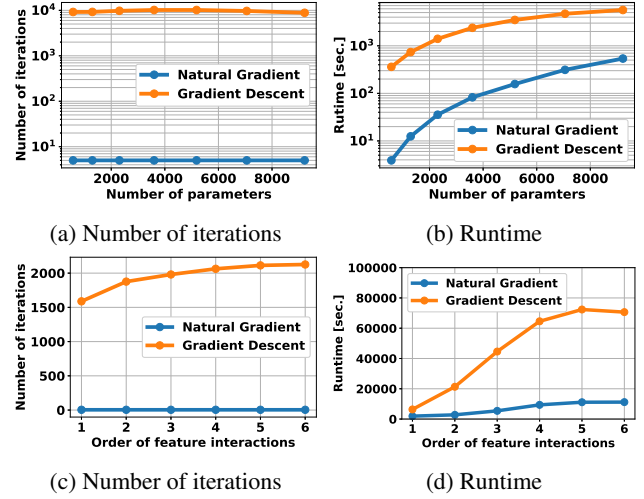


Figure 4: Experimental analysis of the scalability of number of parameters and higher-order features in the model for both natural gradient approach and gradient descent.

of parameters $|\mathbf{Z}|$, $|\mathcal{A}|$ remain this same. Since the complexity of natural gradient is $O(|\mathbf{Z}|^3 + |\mathcal{A}|^3 + |\Omega||S|)$, increasing the size of the input is unlikely to increase the runtime significantly unless $|\Omega||S|$ is greater than $|\mathbf{Z}|$.

Our experimental analysis in Figure 4 shows that our model scales linearly for both natural gradient and gradient descent when increasing the order of interactions in our model. This is because for practical application it is unlikely that $|\mathcal{A}| > |\mathbf{Z}|$. The difference between the runtime for natural gradient and gradient descent is much larger as the order of interactions increased.

Conclusion

We have proposed a novel blind source separation (BSS) method, called *Information Geometric Blind Source Separation* (IGBSS). We have formulated our approach using the information geometric formulation of the log-linear model, which enables us to introduce a hierarchical structure into its sample space to achieve BSS. We have theoretically shown that IGBSS has desirable properties for BSS such as uniquely recovering source signals. It solves the convex optimization problem by minimizing the KL divergence from mixed signals to source signals to find the global optimal.

We then experimentally shown that IGBSS recovers images closer to the ground truth than independent component analysis (ICA), dictionary learning (DL) and non-negative matrix factorization (NMF). Thanks to the flexibility of the hierarchical structure, IGBSS is able to separate signals with complex interactions such as higher-order interactions.

Our work has provided an alternative formulation for BSS, which is supported with strong theoretical guarantees and experimental results to provide a better recovery of the source signal. Our approach is flexible and requires less assumptions than all alternative approaches to be applied to various real world applications such as medical imaging, signal processing, and image processing.

References

- [Amari 1998] Amari, S.-I. 1998. Natural gradient works efficiently in learning. *Neural computation* 10(2):251–276.
- [Amari 2009] Amari, S. 2009. Information geometry and its applications: Convex function and dually flat manifold. In Nielsen, F., ed., *Emerging Trends in Visual Computing: LIX Fall Colloquium, ETVC 2008, Revised Invited Papers*. Springer. 75–102.
- [Amari 2016] Amari, S. 2016. *Information Geometry and Its Applications*. Springer.
- [Bell and Sejnowski 1995] Bell, A. J., and Sejnowski, T. J. 1995. An information-maximization approach to blind separation and blind deconvolution. *Neural computation* 7(6):1129–1159.
- [Berne et al. 2007] Berne, O.; Joblin, C.; Deville, Y.; Smith, J.; Rapacioli, M.; Bernard, J.; Thomas, J.; Reach, W.; and Abergel, A. 2007. Analysis of the emission of very small dust particles from spitzer spectro-imagery data using blind signal separation methods. *Astronomy & Astrophysics* 469(2):575–586.
- [Boutsidis and Gallopoulos 2008] Boutsidis, C., and Gallopoulos, E. 2008. Svd based initialization: A head start for nonnegative matrix factorization. *Pattern recognition* 41(4):1350–1362.
- [Cardoso 1999] Cardoso, J.-F. 1999. High-order contrasts for independent component analysis. *Neural computation* 11(1):157–192.
- [Censor and Lent 1981] Censor, Y., and Lent, A. 1981. An iterative row-action method for interval convex programming. *Journal of Optimization theory and Applications* 34(3):321–353.
- [Comon 1994] Comon, P. 1994. Independent component analysis, a new concept? *Signal processing* 36(3):287–314.
- [Congedo, Gouy-Pailler, and Jutten 2008] Congedo, M.; Gouy-Pailler, C.; and Jutten, C. 2008. On the blind source separation of human electroencephalogram by approximate joint diagonalization of second order statistics. *Clinical Neurophysiology* 119(12):2677–2686.
- [Davey and Priestley 2002] Davey, B. A., and Priestley, H. A. 2002. *Introduction to lattices and order*. Cambridge university press.
- [Ding, Li, and Jordan 2008] Ding, C. H.; Li, T.; and Jordan, M. I. 2008. Convex and semi-nonnegative matrix factorizations. *IEEE transactions on pattern analysis and machine intelligence* 32(1):45–55.
- [Hyvärinen and Oja 2000] Hyvärinen, A., and Oja, E. 2000. Independent component analysis: algorithms and applications. *Neural networks* 13(4-5):411–430.
- [Isomura and Toyozumi 2016] Isomura, T., and Toyozumi, T. 2016. A local learning rule for independent component analysis. *Scientific reports* 6:28073.
- [Lee and Seung 2001] Lee, D. D., and Seung, H. S. 2001. Algorithms for non-negative matrix factorization. In *Advances in neural information processing systems*, 556–562.
- [Luo and Sugiyama 2019] Luo, S., and Sugiyama, M. 2019. Bias-variance trade-off in hierarchical probabilistic models using higher-order feature interactions. In *Proceedings of the 33rd AAAI Conference on Artificial Intelligence (AAAI-19)*, volume 33, 4488–4495.
- [Murphy 2012] Murphy, K. P. 2012. *Machine learning: a probabilistic perspective*. MIT press.
- [Olshausen and Field 1997] Olshausen, B. A., and Field, D. J. 1997. Sparse coding with an overcomplete basis set: A strategy employed by v1? *Vision research* 37(23):3311–3325.
- [Pearson 1901] Pearson, K. 1901. Liii. on lines and planes of closest fit to systems of points in space. *The London, Edinburgh, and Dublin Philosophical Magazine and Journal of Science* 2(11):559–572.
- [Scholz et al. 2005] Scholz, M.; Kaplan, F.; Guy, C. L.; Kopka, J.; and Selbig, J. 2005. Non-linear pca: a missing data approach. *Bioinformatics* 21(20):3887–3895.
- [Sugiyama, Nakahara, and Tsuda 2016] Sugiyama, M.; Nakahara, H.; and Tsuda, K. 2016. Information decomposition on structured space. In *2016 IEEE International Symposium on Information Theory (ISIT)*, 575–579.
- [Sugiyama, Nakahara, and Tsuda 2017] Sugiyama, M.; Nakahara, H.; and Tsuda, K. 2017. Tensor balancing on statistical manifold. In *Proceedings of the 34th International Conference on Machine Learning (ICML)*, volume 70 of *Proceedings of Machine Learning Research*, 3270–3279.
- [Sugiyama, Nakahara, and Tsuda 2018] Sugiyama, M.; Nakahara, H.; and Tsuda, K. 2018. Legendre decomposition for tensors. In *Advances in Neural Information Processing Systems 31*, 8825–8835.
- [Vigário et al. 1998] Vigário, R.; Jousmäki, V.; Hämmäläinen, M.; Hari, R.; and Oja, E. 1998. Independent component analysis for identification of artifacts in magnetoencephalographic recordings. In *Advances in neural information processing systems*, 229–235.
- [Xu, Caramanis, and Sanghavi 2010] Xu, H.; Caramanis, C.; and Sanghavi, S. 2010. Robust pca via outlier pursuit. In *Advances in Neural Information Processing Systems*, 2496–2504.
- [Zou, Hastie, and Tibshirani 2006] Zou, H.; Hastie, T.; and Tibshirani, R. 2006. Sparse principal component analysis. *Journal of computational and graphical statistics* 15(2):265–286.

Appendix: Supplementary Material

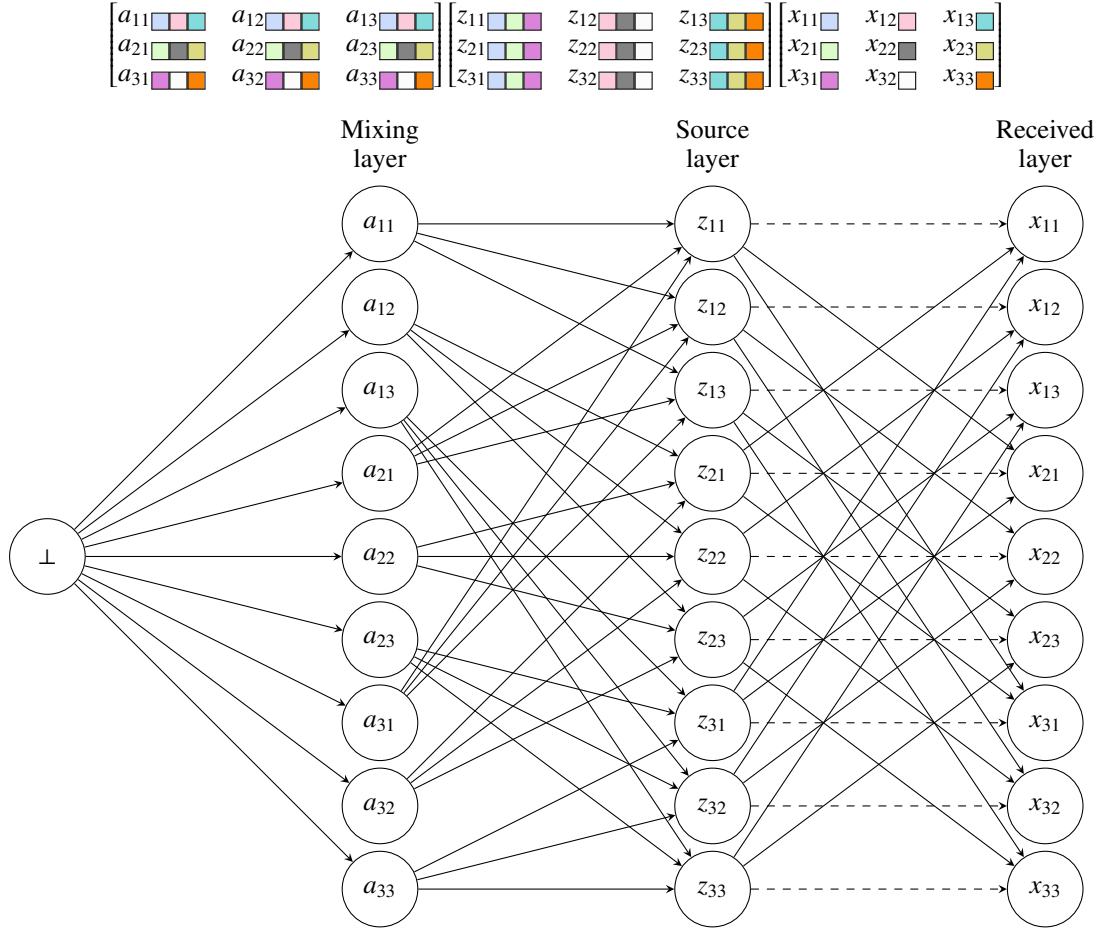


Figure 5: An example of our sample space. The color blocks in the matrix shows corresponding nodes which are in the lower set of a node in the received layer x_{lm} . The dashed line shows removed partial orders to allow for learning.

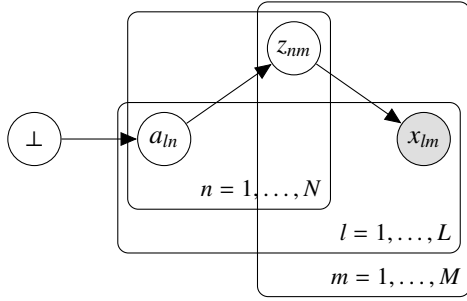
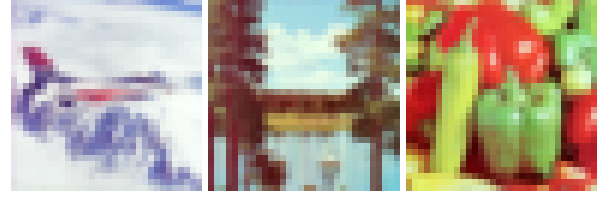


Figure 6: Graph representation of the information geometric formulation of blind source separation using plate notation for the fully connected configuration without edge removal.



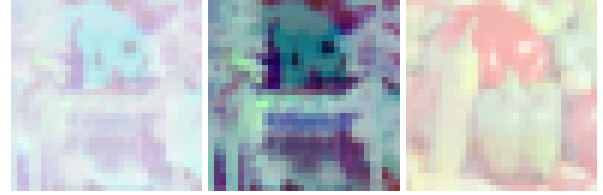
(a) Source signal (ground truth).



(b) Received signal (input).



(c) Reconstructed signal using IGBSS.



(d) Reconstructed Signal using FastICA.

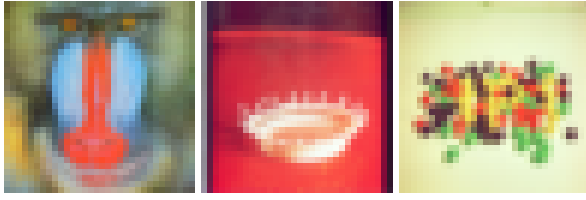


(e) Reconstructed signal using dictionary learning with positive dictionary and positive code.

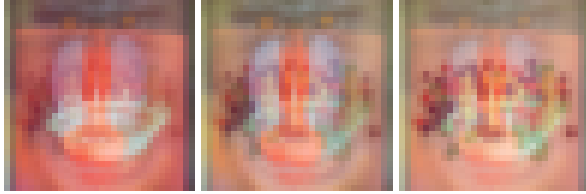


(f) Reconstructed signal using non-negative matrix factorization.

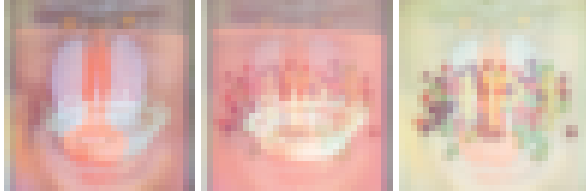
Figure 7: Experiment 1. Number of source signal: 3, order of interaction: 2, Number of mixed signal: 3.



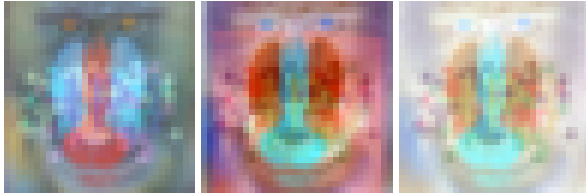
(a) Source signal (ground truth).



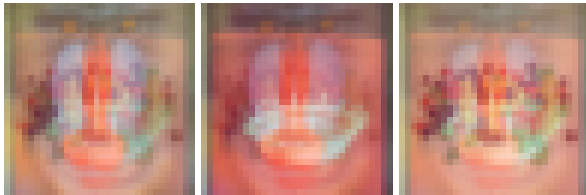
(b) Received signal (input).



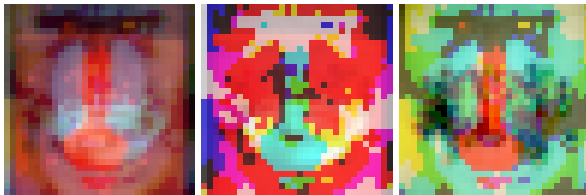
(c) Reconstructed signal using IGBSS.



(d) Reconstructed Signal using FastICA.

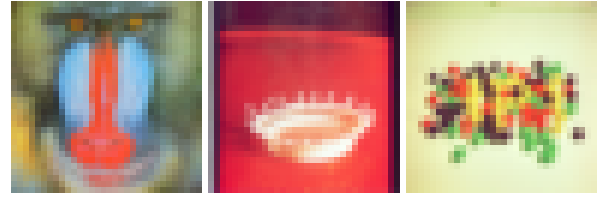


(e) Reconstructed signal using dictionary learning with positive dictionary and positive code.

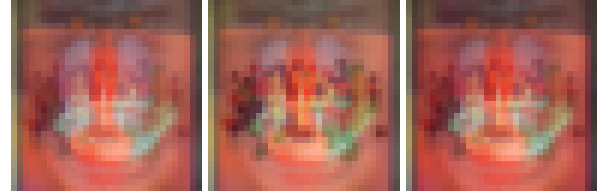


(f) Reconstructed signal using non-negative matrix factorization.

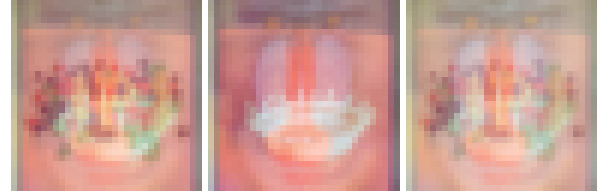
Figure 8: Experiment 2. Number of source signal: 3, order of interaction: 1, Number of mixed signal: 3.



(a) Source signal (ground truth).



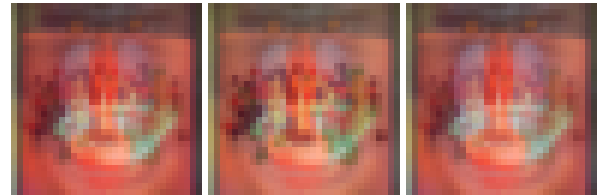
(b) Received signal (input).



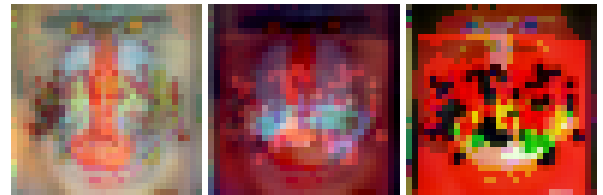
(c) Reconstructed signal using IGBSS.



(d) Reconstructed Signal using FastICA.

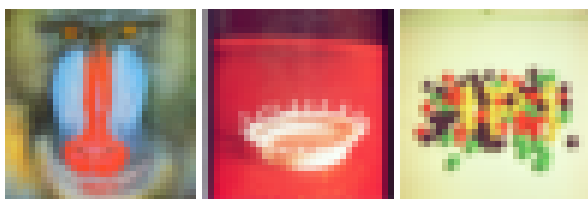


(e) Reconstructed signal using dictionary learning with positive dictionary and positive code.

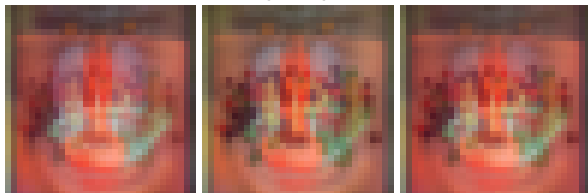


(f) Reconstructed signal using non-negative matrix factorization.

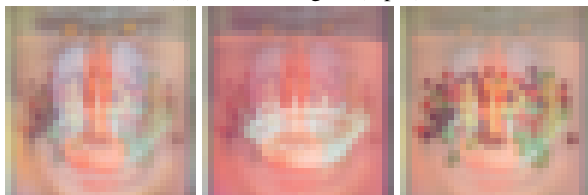
Figure 9: Experiment 2. Number of source signal: 3, order of interaction: 2, Number of mixed signal: 3.



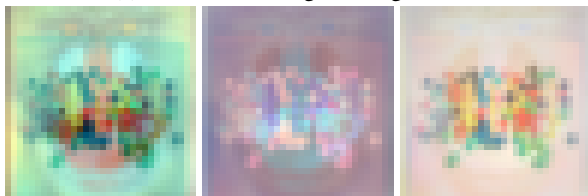
(a) Source signal (ground truth).



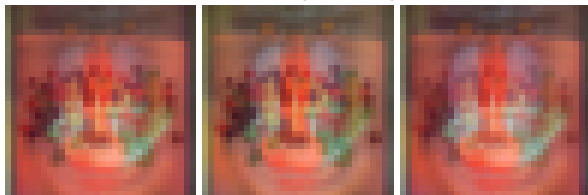
(b) Received signal (input).



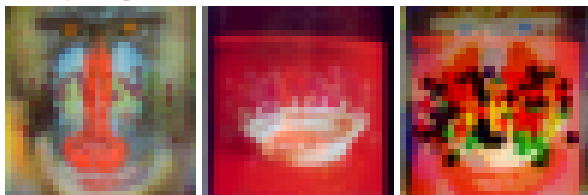
(c) Reconstructed signal using IGBSS.



(d) Reconstructed Signal using FastICA.

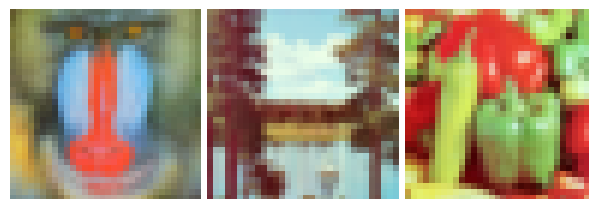


(e) Reconstructed signal using dictionary learning with positive dictionary and positive code.

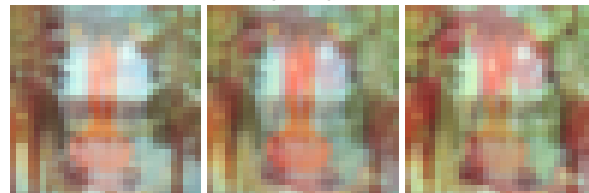


(f) Reconstructed signal using non-negative matrix factorization.

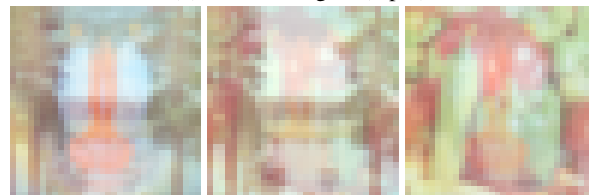
Figure 10: Experiment 2. Number of source signal: 3, order of interaction: 3, Number of mixed signal: 3.



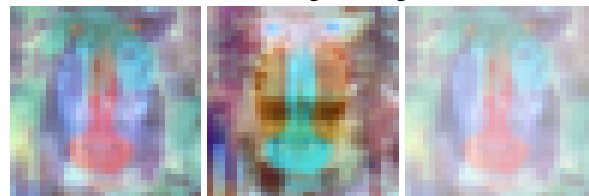
(a) Source signal (ground truth).



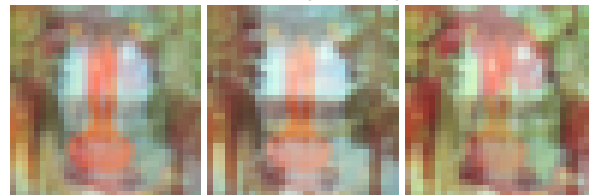
(b) Received signal (input).



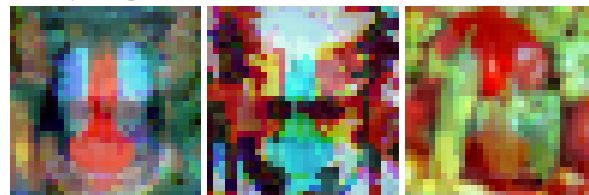
(c) Reconstructed signal using IGBSS.



(d) Reconstructed Signal using FastICA.

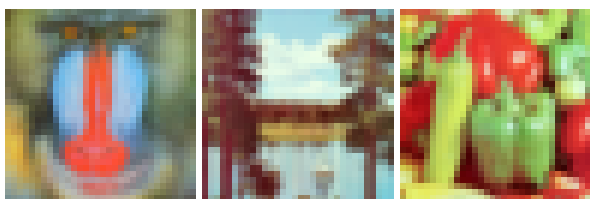


(e) Reconstructed signal using dictionary learning with positive dictionary and positive code.



(f) Reconstructed signal using non-negative matrix factorization.

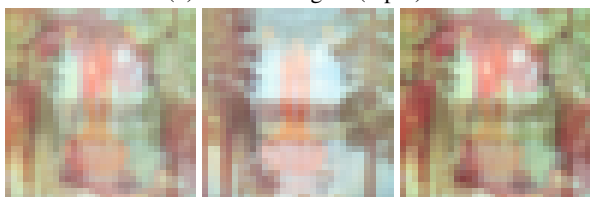
Figure 11: Experiment 3. Number of source signal: 3, order of interaction: 1, Number of mixed signal: 3.



(a) Source signal (ground truth).



(b) Received signal (input).



(c) Reconstructed signal using IGBSS.



(d) Reconstructed Signal using FastICA.

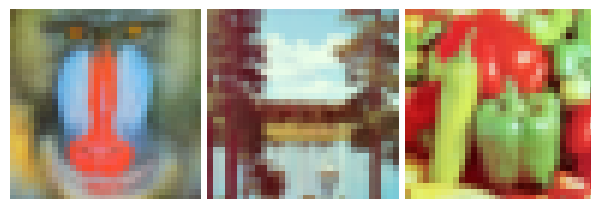


(e) Reconstructed signal using dictionary learning with positive dictionary and positive code.



(f) Reconstructed signal using non-negative matrix factorization.

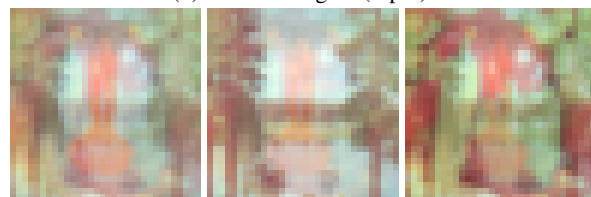
Figure 12: Experiment 3. Number of source signal: 3, order of interaction: 2, Number of mixed signal: 3.



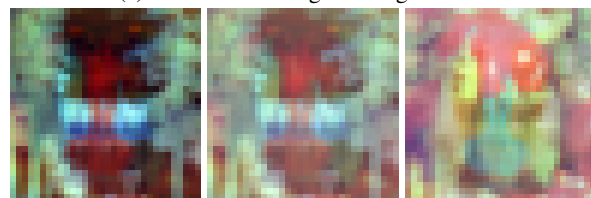
(a) Source signal (ground truth).



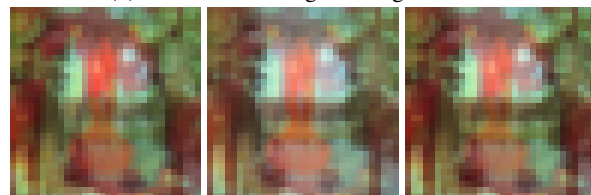
(b) Received signal (input).



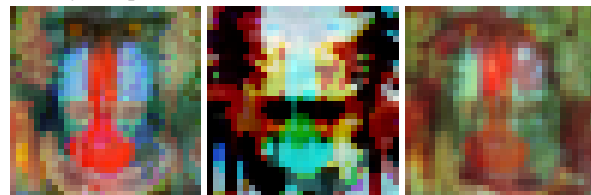
(c) Reconstructed signal using IGBSS.



(d) Reconstructed Signal using FastICA.



(e) Reconstructed signal using dictionary learning with positive dictionary and positive code.



(f) Reconstructed signal using non-negative matrix factorization.

Figure 13: Experiment 3. Number of source signal: 3, order of interaction: 3, Number of mixed signal: 3.